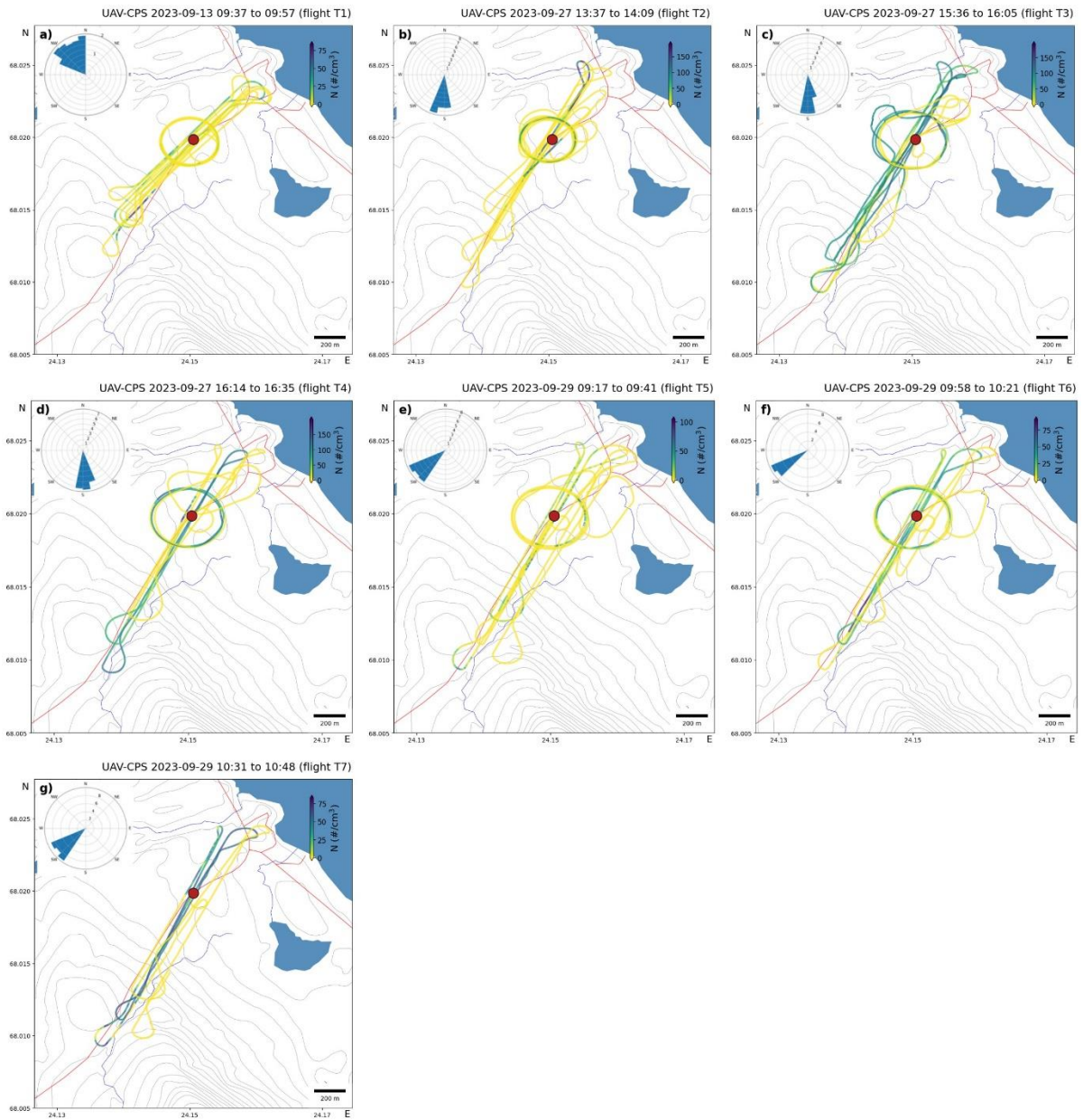


1 SUPPLEMENT

2

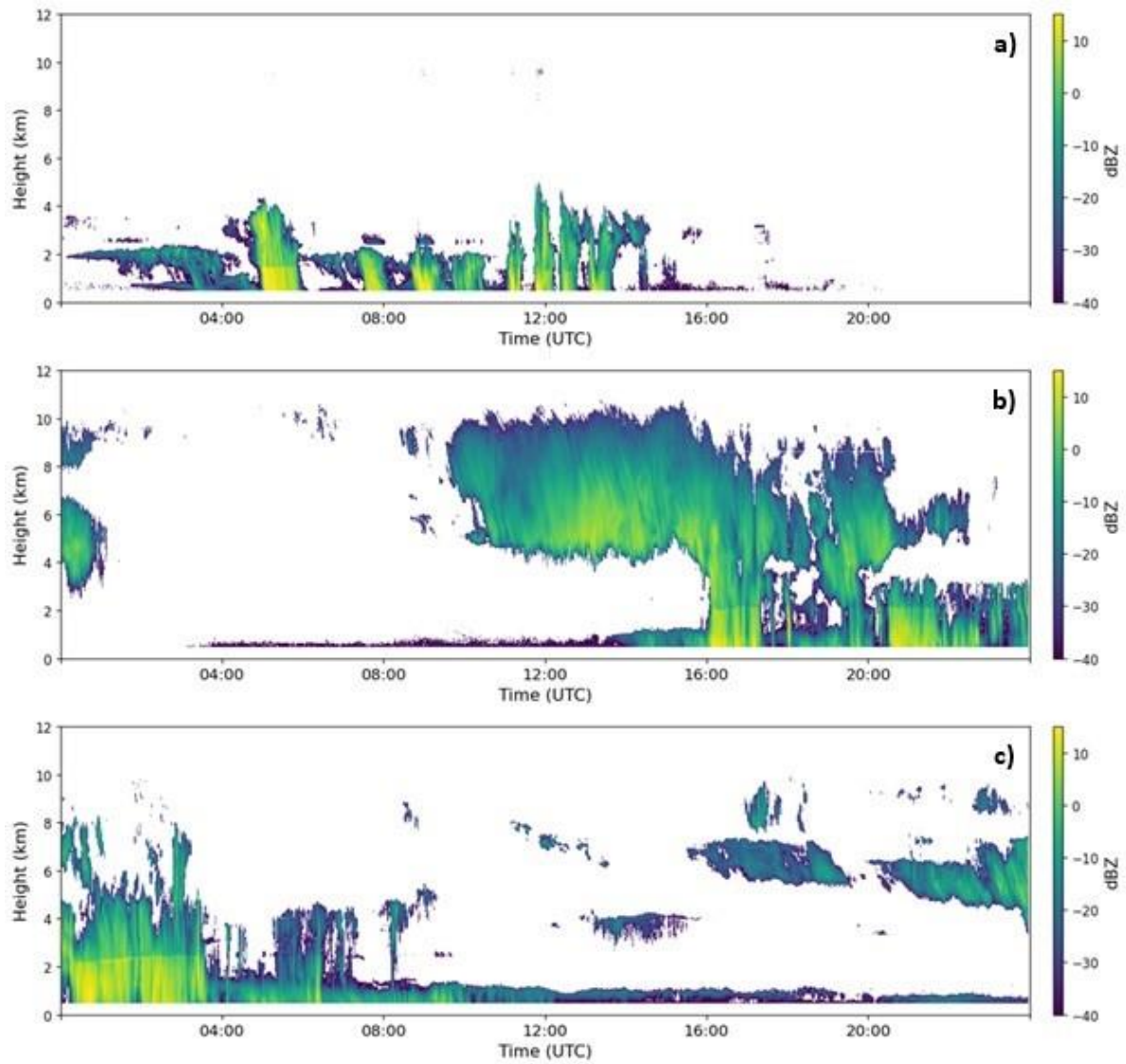


3

4 Figure S1. The UAV-CPS flight paths and cloud droplet number concentrations,
5 including the prevailing wind rose.

6

7

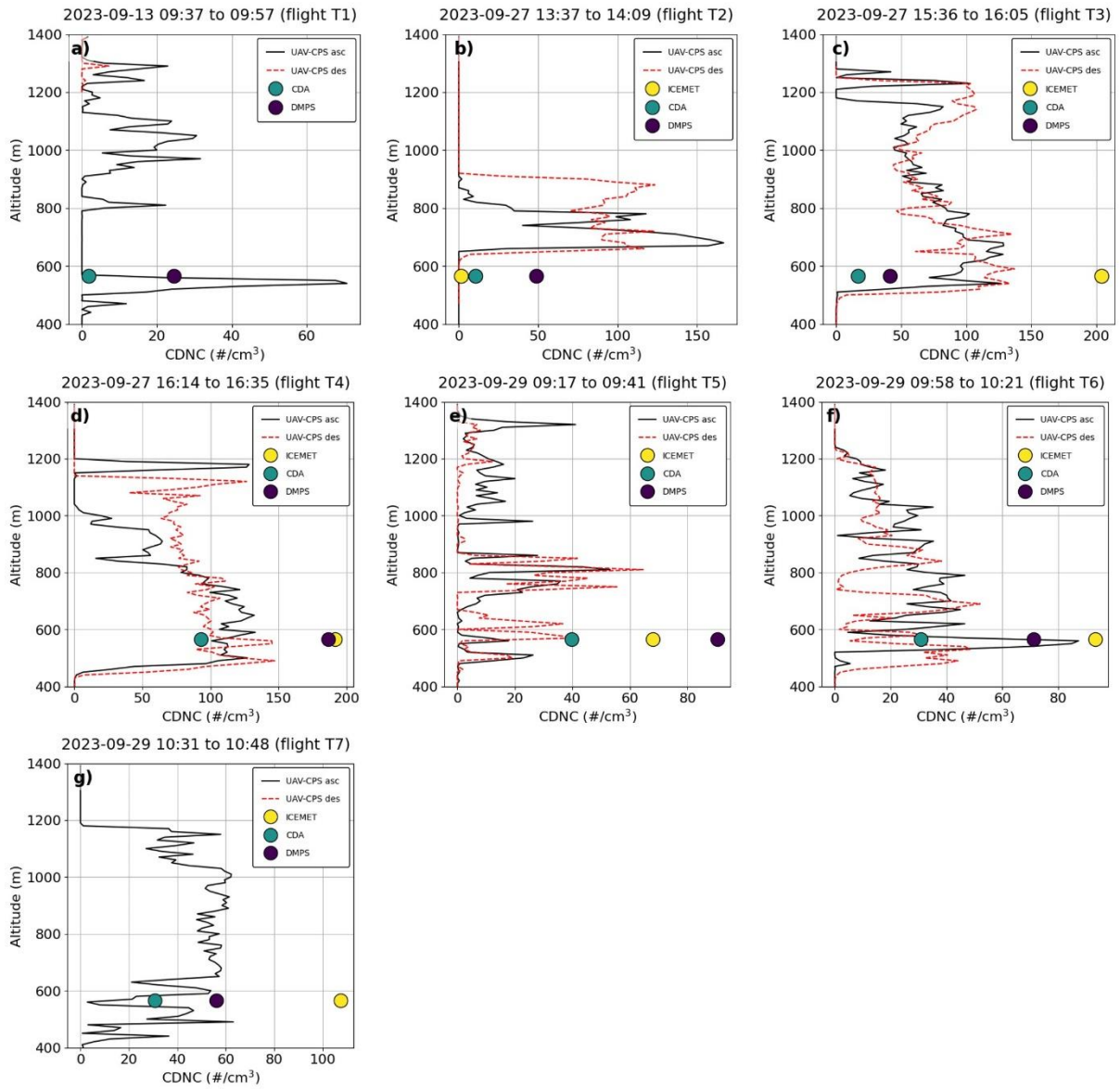


8

9 Figure S2. Cloudnet radar reflectivity factor product, Kenttäröva, Finland, from a) 13
 10 September (O'Connor, 2024a), b) 27 September 2023 (O'Connor, 2024b) and c) 29
 11 September 2023 (O'Connor, 2024c).

12

13

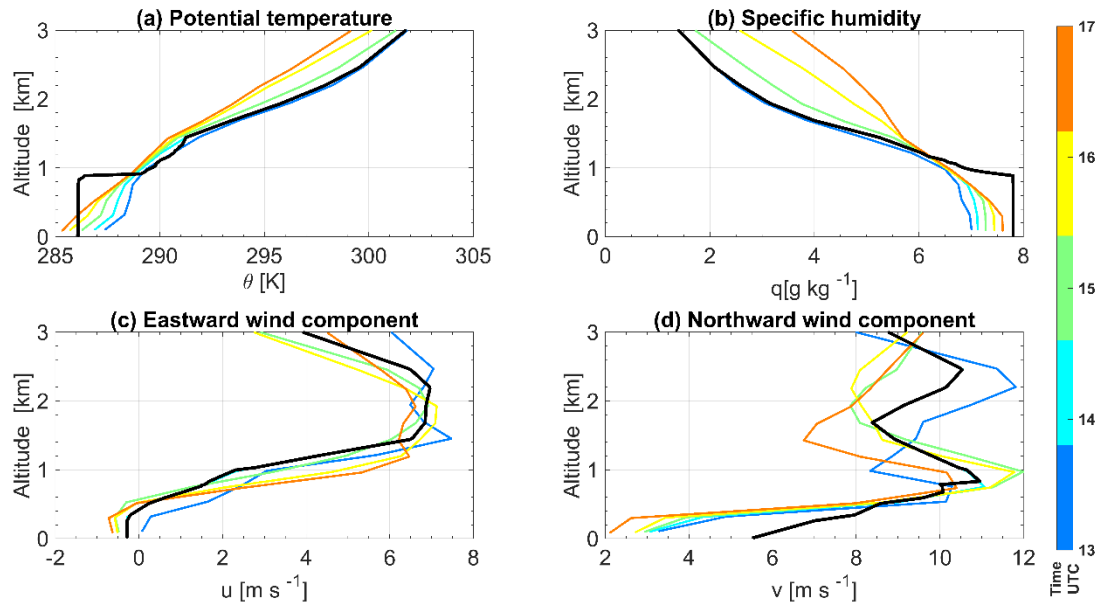


14

15 Figure S3. Cloud droplet number concentration during flights T1-T7.

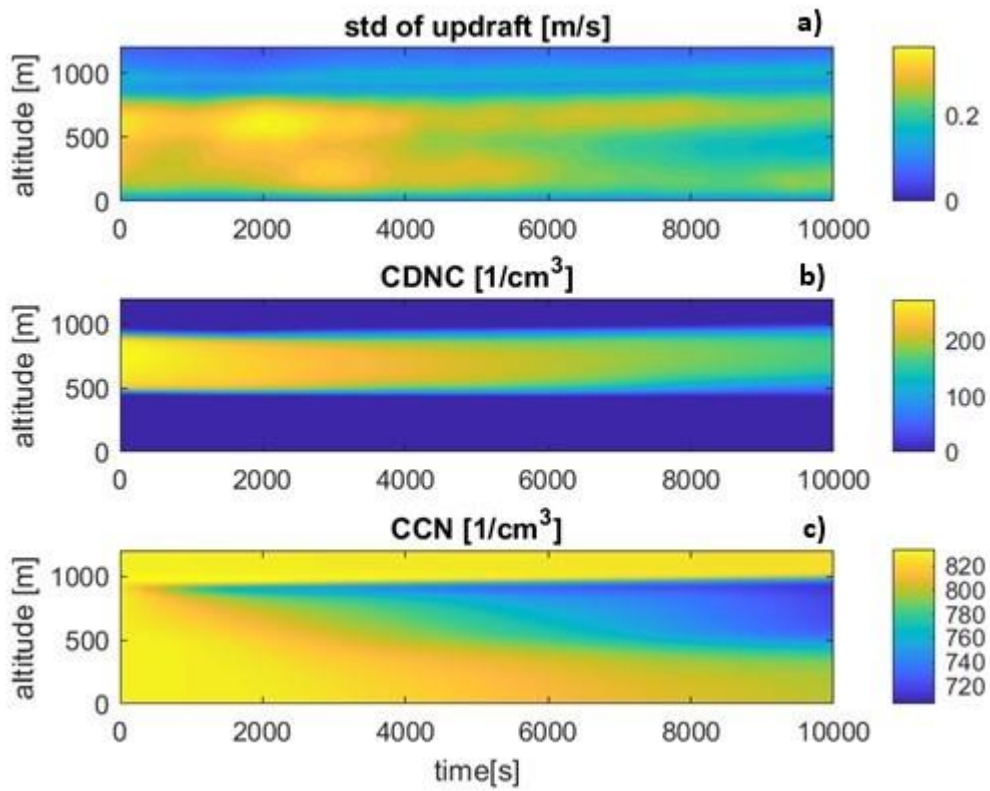
16

17



18
 19 Figure S4. Vertical profiles of atmospheric variables used to define the initial
 20 thermodynamic state in UCLALES-SALSA simulations of the cloud case of 27 September
 21 2025. Data derived from ECWMF-ERA 5 reanalyzed hourly data on pressure levels
 22 (Hersbach et al. 2023)

23
 24
 25
 26



27

28 Figure S5. Average vertical profiles from UCLALES-SALSA simulations of the cloud case
 29 of 27 September 2025. a) standard deviation of updraft velocity, b) cloud droplet
 30 number concentration, c) concentration of aerosol particles (including the interstitial
 31 particles from cloud droplets) with diameter larger than 50 micrometers.

32 UCLALES-SALSA simulations

33 The influence of the overlaying ice clouds was accounted for in calculations of radiative
34 transfer including an ice layer of 100 gm^{-2} with vertically constant effective radius of 40
35 μm . Figure S4 shows the sounding profiles to define the initial atmospheric
36 thermodynamic state. Aerosols particles are distributed over ten size bins from 3 nm to
37 $10 \mu\text{m}$ in dry diameter, cloud droplets are assigned to the last seven aerosol bins
38 depending on the activation diameter. Precipitation droplets are distributed over ten size
39 bins with minimum diameter of $20 \mu\text{m}$ separated by a constant volume ratio of 2. The
40 model was initialized with vertically constant aerosol loading comprising particles
41 composed of pure organic carbon in a bimodal lognormal size distribution (geometric
42 mean diameter of $0.058 \mu\text{m}$ and $0.178 \mu\text{m}$; geometric standard deviation of 1.56 and
43 1.34; and total number concentration of 715 mg^{-1} and 143 mg^{-1}). The surface forcing was
44 constant along the simulation time with sensible heat and latent heat fluxes of 5 Wm^{-2}
45 and 20 Wm^{-2} , respectively.

46

47 DATA AVAILABILITY

48 The Cloudnet data used in this study are generated by the Aerosol, Clouds and Trace
49 Gases Research Infrastructure (ACTRIS) and are available from the ACTRIS Data Centre
50 using the links given in the references.

51

52 ACKNOWLEDGEMENTS

53 We acknowledge ACTRIS and Finnish Meteorological Institute for providing the data set
54 which is available for download from <https://cloudnet.fmi.fi>. We acknowledge ECMWF
55 for providing IFS model data.

56

57 REFERENCES

58 O'Connor, E.: Categorize data from Kenttäröva on 13 September 2023, ACTRIS Cloud
59 remote sensing data centre unit (CLU),
60 <https://hdl.handle.net/21.12132/1.926e86e1dda743f1>, 2024a.

61 O'Connor, E.: Categorize data from Kenttäröva on 27 September 2023. ACTRIS Cloud
62 remote sensing data centre unit (CLU).
63 <https://hdl.handle.net/21.12132/1.d8daf091a8554971>, 2024b.

64 O'Connor, E.: Categorize data from Kenttäröva on 29 September 2023. ACTRIS Cloud
65 remote sensing data centre unit (CLU).
66 <https://hdl.handle.net/21.12132/1.775e5abfe6ad4022>, 2024c.